DOI: 10.61782/fa.2025.0423

FORUM ACUSTICUM EURONOISE 2025

GEOMETRICAL OPTIMISATION OF AN ACOUSTIC METAMATERIAL FOR LOW-FREQUENCY SOUND ABSORPTION

María Luisa López-Ibáñez[1*] **Aurora Melis**[1] **Jorge Muñoz-Paniagua**[2]
César Díaz[3] **Eduardo Latorre-Iglesias**[1]
[1] Grupo de Acústica Arquitectónica, Escuela Técnica Superior de Arquitectura, Universidad Politécnica de Madrid, Spain
[2] E.T.S. Ingenieros Industriales, Universidad Politécnica de Madrid, Spain
[3] Grupo de Tratamiento de Imágenes, Information Processing and Telecommunications Center, Universidad Politécnica de Madrid, Spain

ABSTRACT

An acoustic metamaterial is developed as a combination of microperforated panels backed by a cavity with several Helmholtz resonators, aimed to achieve high absorption at low frequencies while maintaining a limited size. Its design is optimised using three numerical methods: Markov chain Monte Carlo, genetic algorithms, and neural networks. The optimization is based on an analytical description of the system, building the equivalent electro-acoustic circuit and solving for normal sound incidence. The free parameters during the optimization processes are related to the geometry of the components: the distance between microperforations (which determines the porosity of the microperforated panels), the depth of the back cavities, and the neck length and diameter of the Helmholtz resonators. For all methods, the cost function quantifies the difference between an ideal absorption coefficient, $\alpha_0 = 1$, and the absorption coefficient of the system in the frequency range considered (between 100 Hz and 1500 Hz). The solutions obtained are validated using the finite element method in COMSOL Multiphysics. Optimization approaches are compared in terms of computational cost and performance of the solution.

*__Corresponding author__: ml.lopez@upm.es.

Keywords: *Acoustic metamaterials, Sound absorption, Monte Carlo, Genetic algorithms, Neural networks*

1. INTRODUCTION

Sound absorption by resonant acoustic metamaterials (AMM) has gained increasing attention in the reduction of low-frequency noise as an alternative to conventional solutions such as porous materials. Porous materials have been largely used, but their application in confined spaces, when targeting low frequencies, is very challenging because a sizeable thickness is needed to be effective.

To overcome these limitations, and thanks to the development of affordable and fast 3-D printing technologies, the design of resonant AMM has become highly convenient. Helmholtz Resonators (HR) are typically used for noise absorption at specific frequencies adjusting their geometrical parameters (cavity volume and neck length and cross-sectional surface area). Microperforated panes (MPP) are also commonly used in sound absorption applications as they provide relatively low-frequency sound absorption with a limited thickness, and in a wider frequency range than that obtained with HRs. Their absorption frequency range and amplitude depend on the chosen geometrical parameters, namely microperforation size, porosity factor and distance between the microperforated panel and the rigid backing. Combining HRs with MPPs, large sound absorption in a wide frequency range, comprising low and middle frequencies, can be achieved. It is desirable, however, to explore different geometries and select

the one with the best performance.

If an analytical description of the absorber is available, this can be done by optimization routines such as Monte Carlo methods (MC), genetic algorithms (GA), or neural networks (NN). These methods can be classified as zeroth-order algorithms, as MC and GA, which do not involve derivatives of any analytical function, or first-order methods, as NN, which typically relies on gradient descent.

In this work, a solution based on a combination of 16 HRs and 4 MPPs is proposed to reduce low-frequency noise between 100 Hz and 1500 Hz. The designs obtained are validated using the finite element method in COMSOL Multiphysics. The aim is to assess differences among solutions derived from different methods, but also among computational costs, so the appropriate algorithm can be applied to optimize future designs.

The paper is organized as follows: the analytical description of the absorber is presented in Section 2. In Section 3, the constraints considered for the numerical optimization are collected and the main features of each method summarized. Section 4 contains a brief description of the FEM simulation in COMSOL Multiphysics. In Section 5, the results of the optimizations and numerical simulations are shown and discussed. Finally, our conclusions are presented in Section 6.

2. ANALYTICAL DESCRIPTION OF THE ABSORBER

The analytical description of the system is made in terms of the equivalent electro-acoustic circuit, where each element is represented by its corresponding acoustic impedance. The total impedance of the system, Z_{tot}, is calculated by summing the individual impedances as corresponds (in parallel or in series). The absorption coefficient at a given frequency can then be written in terms of Z_{tot} as

$$\alpha(f) \;=\; 1 - \left| \frac{Z_{\text{tot}}(f) - Z_0}{Z_{\text{tot}}(f) + Z_0} \right|^2 , \qquad (1)$$

where $Z_0 = \rho_0\, c_0$ is the characteristic air impedance, with $\rho_0 = 1.24\,\text{kg/m}^3$ the air density and $c_0 = 343\,\text{m/s}$ the speed of sound in air at $20\,^\circ C$.

In our case, the total impedance of the system is computed considering four MPPHR blocks arranged in parallel. Each MPPHR block consists of a micro-perforated panel (MPP) in series with four Helmholtz resonators (HR), see Fig. 1. The cross-sectional area of the HRs is $\ell_{\text{HR}} \times \ell_{\text{HR}} \equiv 30 \times 30\,\text{mm}^2$ so that each MPP panel is $60 \times 60\,\text{mm}^2$. The neck lengths and diameters of HRs within an MPPHR block are different among them, but the same set of four diameters and lengths is considered from one block to another. In effect, there are sixteen distinct HRs because the cavity does change from one MPPHR block to another.

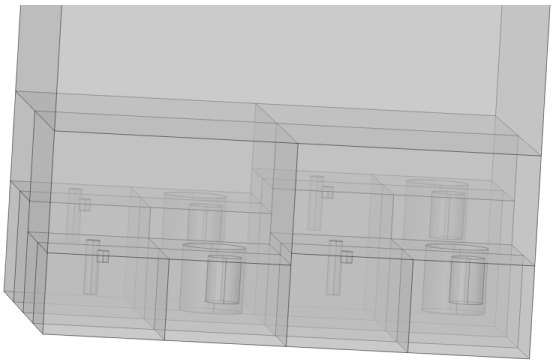

Figure 1. Structure of the proposed acoustic metamaterial. Four MPPs can be distinguised in the upper part of the figure as square surfaces; below each of them, four HRs in series.

The acoustic behaviour of each MPPHR block is described by an impedance Z_m, where $m = 1, ..., 4$ refers to the $m-$block. Then, the total impedance of the AMM is given by the parallel sum of the MPPHR impedances [1]

$$Z_{\text{tot}}^{-1}(f) \;=\; \sum_{m=1}^{4} \frac{S_m}{Z_m(f)}, \quad S_m = 1/4 \qquad (2)$$

with

$$Z_m(f) \;=\; Z_{\text{MPP}_m}(f) + \left(\frac{1}{Z_{\text{C}_m}(f)} + \sum_{n=1}^{4} \frac{S_{mn}}{Z_{\text{HR}_{mn}}(f)} \right)^{-1} \qquad (3)$$

The factor $S_m = 1/4$ in Eq.(2) is the ratio between the cross-sectional area of each MPP versus the total system. Similarly, S_{mn} in Eq.(3) refers to the relation between the cross sectional area of the $n-$HR compared to the $m-$MPP in that block. Finally, Z_{MPP_m}, Z_{C_m}, and $Z_{\text{HR}_{mn}}$ in Eq.(3) are the impedances associated with the $m-$MPP, the backed cavity, and the $n-$ HR in the $m-$ensemble.

Regarding MPP, its impedance can be divided into

real and imaginary parts such as

$$Z_{\mathrm{MPP}_m}(f) \;=\; Z_0\left[R_{\mathrm{MPP}_m}(f) + j\,X_{\mathrm{MPP}_m}(f)\right] \quad (4)$$

where

$$R_{\mathrm{MPP}_m}(f) = \frac{32\,\eta}{Z_0}\frac{t_m}{\sigma_m\,d_m^2}\left(\sqrt{1+\frac{k_m^2(f)}{32}}+\frac{\sqrt{2}\,k_m(f)}{8}\frac{d_m}{t_m}\right), \quad (5)$$

$$X_{\mathrm{MPP}_m}(f) = \frac{2\pi f}{c_0}\frac{t_m}{\sigma_m}\left(1+\frac{1}{\sqrt{9+k_m^2(f)/2}}+0.85\,\frac{d_m}{t_m}\right), \quad (6)$$

with $\eta = 1.84\times10^{-5}\,\mathrm{Pa\,s^{-1}}$ the dynamic viscosity of air, $d_m = t_m = 0.5\,\mathrm{mm}$ the diameter of the microperforations and the thickness of the panel, k_m approximated as

$$k_m(f) \;=\; \frac{d_m}{2}\sqrt{2\pi f\,\frac{\rho_0}{\eta}}, \quad (7)$$

and σ_m the porosity of the MPP, defined as the ratio of void volume and total volume. In this case, σ_m can be expressed in terms of the distance between microperforations, D_m, and their diameter, d_m, as

$$\sigma_m \;=\; \frac{\pi d_m^2}{4\,D_m^2}, \quad (8)$$

The impedance of the cavity between the MPP and the resonators is purely imaginary and is simply given by

$$Z_{\mathrm{C}_m}(f) \;=\; -j\,Z_0\,\cot\left[\frac{2\pi f}{c_0}l_{I_m}\right], \quad (9)$$

where l_{I_m} is the depth of the cavity. The HR impedance has also real and imaginary parts so that

$$Z_{\mathrm{HR}_{mn}}(f) \;=\; Z_0\left[R_{\mathrm{HR}_n}(f) + j\,X_{\mathrm{HR}_{mn}}(f)\right] \quad (10)$$

where

$$R_{\mathrm{HR}_n}(f) = \frac{\sqrt{16\pi\,\eta\,\rho_0\,f}}{Z_0\,\varepsilon_n}\left(1+\frac{l_{N_n}}{d_{N_n}}\right),\ \varepsilon_n = \frac{S_{N_n}}{\ell_{\mathrm{HR}}^2} \quad (11)$$

$$X_{\mathrm{HR}_{mn}}(f) = \frac{2\pi f}{c_0\,\varepsilon_n}\left(l_{N_n}+\delta_{N_n}\right) - \frac{c_0}{2\pi f\,l_{\mathrm{RC}_{mn}}} \quad (12)$$

with l_{N_n} and d_{N_n} the neck length and diameter of the $n-$resonator, $S_{N_n} = \pi\,(d_{N_n}/2)^2$ the section of the neck, $\delta_{N_n} = 0.85\,d_{N_n}$ the correction to the neck length (to take into account radiative effects), and $l_{\mathrm{RC}_{mn}}$ determined by

$$l_{\mathrm{RC}_{mn}}\,[\mathrm{mm}] \;=\; 50 - 2\,t_m - l_{I_m} - \varepsilon_n\left(l_{N_n}+\delta_{N_n}\right) \quad (13)$$

3. NUMERICAL OPTIMIZATION

For optimization, the free parameters correspond to the geometric characteristics of the AMM and they are subjected to the restrictions that are described in the following. First, the total height of the sample must be $50\,\mathrm{mm}$,

$$2\,t_m + l_{I_m} + l_{N_n} + l_{C_{mn}} \;=\; 50\,\mathrm{mm}, \quad \forall\, m,\, n = 1,\ldots,4, \quad (14)$$

with l_{I_m} and $l_{C_{mn}}$ satisfying

$$l_{I_m} \le 35\,\mathrm{mm}, \quad \forall\, m = 1,\ldots,4 \quad (15)$$

$$l_{C_{mn}} \ge 3\,\mathrm{mm}, \quad \forall\, m,\, n = 1,\ldots,4. \quad (16)$$

The diameter of the MPP pores and thickness of the panel must be equal to $0.5\,\mathrm{mm}$ (due to the experimental restrictions),

$$t_m \;=\; d_m \;=\; 0.5\,\mathrm{mm}, \quad \forall\, m = 1,\ldots,4. \quad (17)$$

The diameter of the MPP pores must be always smaller than the distance between microperforations,

$$d_m < D_m, \quad \forall\, m = 1,\ldots,4. \quad (18)$$

Taking Eqs.(14)-(18) into account, the ranges of possible values for the free parameters are:

$$\text{MPP:}\quad l_{I_m} = [10.0,\,30.0]\ \mathrm{mm}, \quad (19)$$

$$D_m = [1.5,\,6.0]\ \mathrm{mm}, \quad \forall\, m = 1,\ldots,4 \quad (20)$$

$$\text{HR:}\quad l_{N_n} = [1.9,\,16.0]\ \mathrm{mm}, \quad (21)$$

$$d_{N_n} = [1.0,\,17.0]\ \mathrm{mm}, \quad \forall\, n = 1,\ldots,4 \quad (22)$$

With respect to the cost function, three scenarios are considered. Initially, the optimization procedure is frequency-blind, which means that all frequencies are equally important. In this case, the cost function is just the squared sum of the differences between the obtained absorption at each frequency and the ideal absorption, $\alpha_0 = 1$:

$$\chi_1^2 = \frac{1}{\sigma_1^2}\sum_{n=1}^{N_f}\left[\alpha\,(f_n) - \alpha_0\right]^2, \quad \sigma_1^2 = N_f \quad (23)$$

However, in order to increase absorption at low frequencies, two alternative frequency-weighted cost functions are also considered:

$$\chi_2^2 = \frac{1}{\sigma_2^2}\sum_{n=1}^{N_f}\frac{1}{f_n}\left[\alpha\,(f_n) - \alpha_0\right]^2, \quad \sigma_2^2 = \sum_{n=1}^{N_f}\frac{1}{f_n} \quad (24)$$

$$\chi_3^2 = \frac{1}{\sigma_3^2}\sum_{n=1}^{N_f}\frac{1}{f_n^2}\left[\alpha\,(f_n) - \alpha_0\right]^2, \quad \sigma_3^2 = \sum_{n=1}^{N_f}\frac{1}{f_n^2} \quad (25)$$

3.1 Markov chain Montecarlo method

The Monte Carlo optimization is divided in two parts consisting of $N_p/3$ and $2N_p/3$ iterations each, where N_p is the total number of repetitions. During the first stage, random combinations of values for the free parameters are uniformly generated considering the intervals in Eqs.(19)-(22). Each combination defines a unique design for the absorber and produces a specific absorption profile in the frequency range of interest. After computing the absorption, as stated in section 2, the cost function is evaluated for this point, $\chi^2_{i,n}$, and compared to the value obtained for the last candidate to best fit point (BFP), χ^2_i. The candidate to BFP is replaced by the new point when it is satisfied:

$$e^{\chi^2_i - \chi^2_{i,n}} > \text{Random}\,[0,\,1]\,, \tag{26}$$

where $\text{Random}\,[0,\,1]$ stands for a random number between zero and one, following a uniform distribution. From Eq.(26), notice that the best solution is not always kept as BFP. However, in this preliminary part of the optimization, this feature is desirable since it facilitates evading local minima and, consequently, a more effective scanning of the parameter space.

The second part of the optimization starts with the best solution of the previous part (which may not be the current BFP). A Markov-chain procedure is now followed, where the new solution is generated around the coordinates of the BFP, considering Gaussian distributions centered at the BFP and with a standard deviation equal to the 1% of the center value. In this case, the BFP is replaced by the new point only when $\chi^2_i < \chi^2_{i,n}$.

3.2 Genetic algorithms

GA, introduced by Holland [2] and developed by Goldberg, [3], are a technique that mimic the mechanics of the natural evolution. Once a population of potential solutions is defined, three operators (selection of the fittest, reproduction or crossover, and mutation) are applied. Iteratively, a new population is generated and better results are obtained until a solution closer to globally optimal solution is reached. The combination of the survival-of-the-fittest concept to eliminate unfit characteristics with a random information exchange and the exploitation of the knowledge contained in old solutions permit GA to effect a search mechanism with efficiency and speed. GA are englobed in zero-order methods, based on direct evaluations of the objective function.

The population size is set as four times the number of design variables, the crossover fraction to 0.6 and the mutation function is the Adaptive Feasible function implemented in MATLAB. The fitness scaling is done by ranking. Elitism is considered and set to 1% of the population size. The convergence rate has not been the same for the three cases, as it took longer (in terms of iterations) to achieve the optimal solution based on χ^2_1 than for the χ^2_2 case. To help the optimization process for the χ^2_1 case, the population size has been changed from four to three times the number of design variables.

3.3 Neural networks

This optimization approach relies on the design of an autoencoder-like NN model [4], with the encoder and decoder defined as follows.

The encoder functions as an inverse model designed to learn the inverse of the analytical function responsible for obtaining the absorption coefficient, see Eq.(14) [5]. For this purpose, a straightforward multilayer perceptron (MLP) is employed. This network takes as input a 1000-point absorption coefficient and features a hidden layer with 1500 neurons, utilizing ReLU activation functions. The output layer, which contains 16 neurons (equivalent to the number of parameters to optimize), uses sigmoid activation functions. The sigmoid functions are adjusted to ensure that the output adheres to the constraints included in Section 3. Consequently, the result is a bottleneck made up of the 16 parameters whose values are subject to optimization.

The decoder directly executes the analytical function without any learnable parameters. By utilizing the bottleneck as an input, it generates an absorption coefficient with one point per frequency within the 100 to 1500 Hz range (i.e., 1401 points).

To train the model, the chi-squared metrics, see Eqs.(23)-(25), serve as loss functions. The training process uses single-sample batches, solely focusing on the desired case where the absorption coefficient equals one across the entire frequency range, and does not use dropout. The rationale lies in the fact that, unlike most applications, our aim is not to create a generalizable model, but rather a completely overfitted one. In addition, an Adam optimizer is applied with an initial learning rate of 10^{-4} over the course of 1500 epochs (iterations).

4. NUMERICAL SIMULATION BY FEM

To corroborate the absorption of our designs predicted by the analytical expressions in Section 2, a finite element

method is implemented by using the software COMSOL Multiphysics. An `Acoustics/Frequency Domain` study is employed, in the frequency range $(100 - 1500)$ Hz and considering a step of 1 Hz. In the simulation, an impedance tube of 1 m long and 10 cm wide with a piston in one extreme and the absorber in the opposite extreme is modeled. The piston is encoded in COMSOL by using the boundary condition `Normal Acceleration`. All the external and internal boundaries are considered hard boundaries, except for the one associated with the MPP for which the `Microperforated Plate/Thin Plate` is chosen. The HR necks are considered as `Narrow Region/Circular Duct`. The mesh is generated as `Physics Controlled`, requiring 5 elements per wavelength. Absorption is computed following the standing wave ratio standard.

5. RESULTS

The geometric parameters of the best solutions obtained for each cost function and by each method are presented in Tabs. 1-3 and Figs. 2-4, where analytical predictions are plotted together with preliminary results obtained by the FEM with COMSOL Multiphysics. Designs obtained from the minimization of χ_1 are plotted in orange, while those from χ_2 are drawn in blue and the ones from χ_3 in green. It is observed that the simulation in COMSOL does not fully agree with the analytical curve for mid and high frequencies, which mainly correspond to the regions where the MPPs act. The authors are currently working on this, and improved results are expected soon.

For the frequency-blind optimization, related to χ_1 in Eq. (23), it is observed that almost identical solutions are produced by all the methods. Some differences arise for the MCMC design in HR1 and HR2, although the value of χ_1 is equal for all the routines. As can be noticed in Tab. 4, the best average absorption in the total interval of frequencies is obtained in this case, with almost no differences among designs.

Regarding χ_2, again the solutions coincide for the GA and NN methods, while the MCMC algorithm differs for HR1 and HR2. The value of the cost function is identical for all the optimization methods. Comparing χ_2 to χ_1, a higher value is obtained. This is in agreement with the fact that the average absorption in the full interval of frequencies is significantly lower than in the previous case, see Tab. 4. However, introducing weights which promote low frequencies has an impact: the absorption in this range, from 100 Hz to 400 Hz, has been increased. This solution can be interesting if low frequencies have a special interest in the applications of our design.

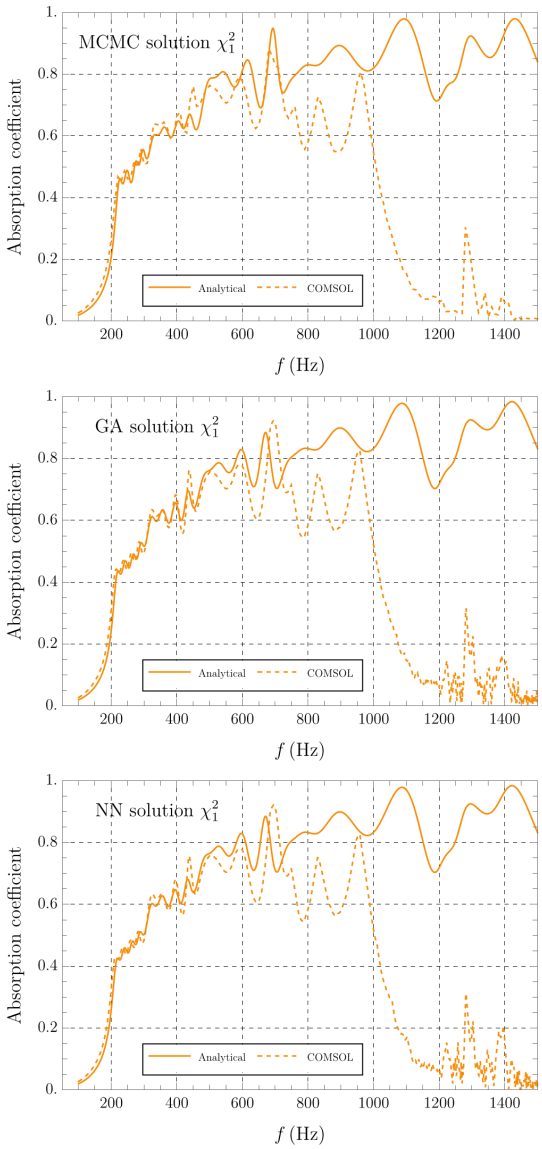

Figure 2. Absorption coefficient between 100 Hz and 1500 Hz for the solutions of χ_1 and χ_2. Analytical predictions are compared to the numerical simulations in COMSOL Multiphysics.

Finally, for χ_3, the designs obtained by the GA and NN methods coincide once more, and the MCMC method differs again in HR1 and HR2. Regarding absorption, as

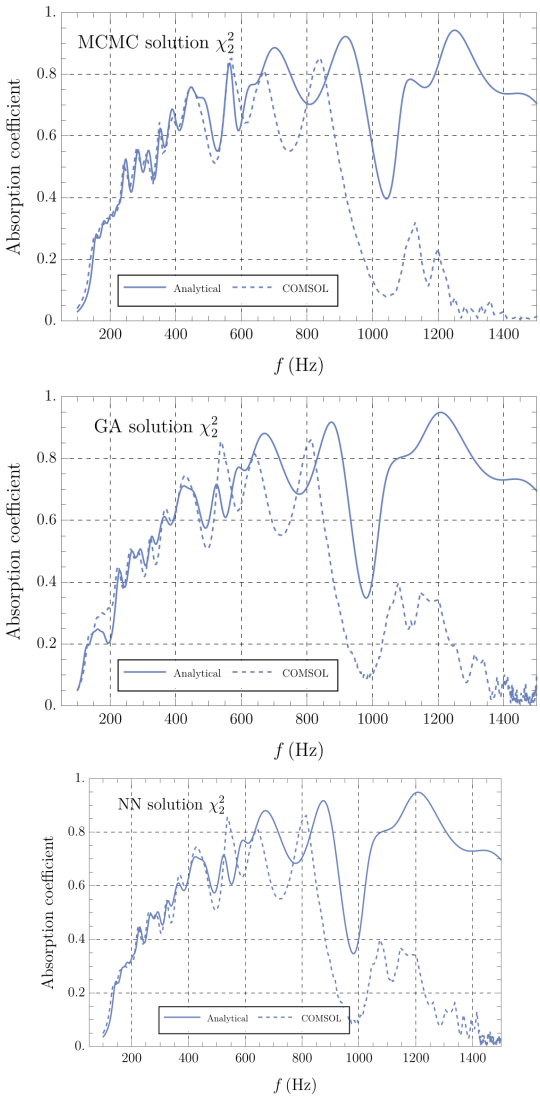

Figure 3. Absorption coefficient between 100 Hz and 1500 Hz for the solutions of χ_1 and χ_2. Analytical predictions are compared to the numerical simulations in COMSOL Multiphysics.

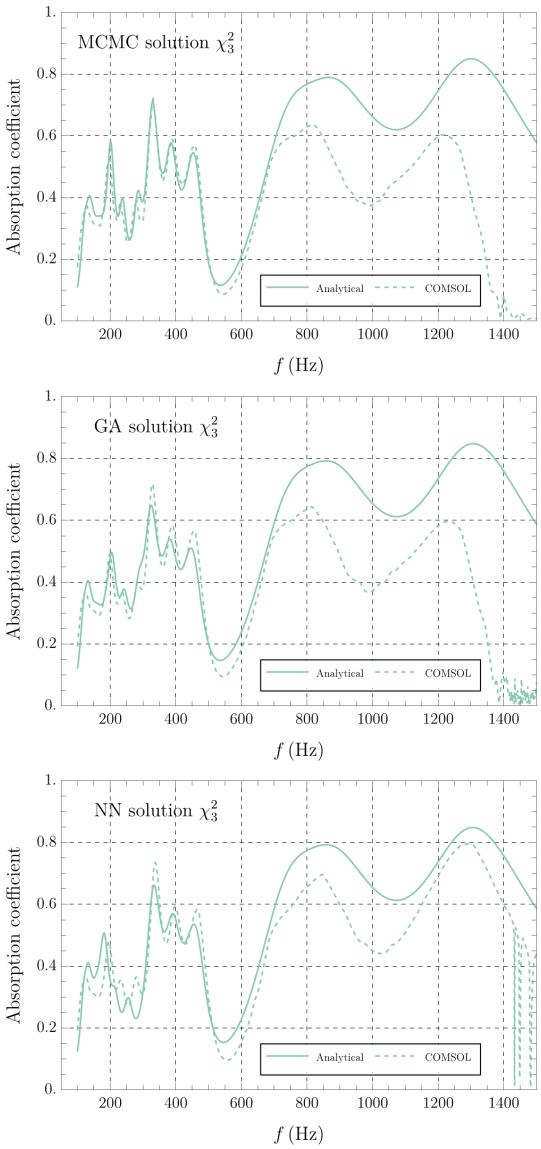

Figure 4. Absorption coefficient between 100 Hz and 1500 Hz for the solutions of χ_3. Analytical predictions are compared to the numerical simulations in COMSOL Multiphysics.

can be observed in Tab. 4, it has been slightly improved in the low-frequency range for the MCMC and GA designs. However, the loss in the total interval of frequencies is so pronounced (with respect to the previous solutions for χ_1 and χ_2) that these designs are discarded. This is in agreement with the fact that the cost function renders a larger value, compared to χ_1 and χ_2. As future work, it is interesting to analyze what power of f_n in σ_i, see Eqs. (24) and (25), optimizes the absorption ratio between low frequencies and the total range.

From Figs. 2-4, it can be seen that very little difference is found among designs obtained with different opti-

Table 1. Best fit points obtained by the MCMC method. Dimensions are given in milimeters.

	$\mathbf{MPP_1}$		$\mathbf{MPP_2}$		$\mathbf{MPP_3}$		$\mathbf{MPP_4}$		$\mathbf{HR_1}$		$\mathbf{HR_2}$		$\mathbf{HR_3}$		$\mathbf{HR_4}$	
	D_1	l_{I_1}	D_2	l_{I_2}	D_3	l_{I_3}	D_4	l_{I_4}	l_{N_1}	d_{N_1}	l_{N_2}	d_{N_2}	l_{N_3}	d_{N_3}	l_{N_4}	d_{N_4}
$\chi_1^2 = \mathbf{0.12}$	3.2	30.0	4.7	27.1	5.8	22.4	6.0	16.2	2.8	2.8	11.2	8.2	13.3	3.3	16.0	15.5
$\chi_2^2 = \mathbf{0.29}$	3.8	30.0	6.0	10.6	6.0	20.3	6.0	26.2	10.0	6.2	14.8	4.2	15.7	2.6	16.0	13.5
$\chi_3^2 = \mathbf{0.40}$	6.0	10.0	6.0	10.2	6.0	21.4	6.0	30.0	4.9	3.8	12.2	2.0	15.2	3.4	15.3	2.0

Table 2. Best fit points obtained by the GA method. Dimensions are given in milimeters.

	$\mathbf{MPP_1}$		$\mathbf{MPP_2}$		$\mathbf{MPP_3}$		$\mathbf{MPP_4}$		$\mathbf{HR_1}$		$\mathbf{HR_2}$		$\mathbf{HR_3}$		$\mathbf{HR_4}$	
	D_1	l_{I_1}	D_2	l_{I_2}	D_3	l_{I_3}	D_4	l_{I_4}	l_{N_1}	d_{N_1}	l_{N_2}	d_{N_2}	l_{N_3}	d_{N_3}	l_{N_4}	d_{N_4}
$\chi_1^2 = \mathbf{0.12}$	3.2	30.0	4.6	26.7	5.8	22.2	6.0	15.7	1.9	4.6	4.6	3.3	11.3	3.0	16.0	15.4
$\chi_2^2 = \mathbf{0.29}$	3.8	30.0	6.0	10.2	6.0	20.6	6.0	26.0	1.9	3.2	9.0	3.1	16.0	2.4	16.0	12.6
$\chi_3^2 = \mathbf{0.40}$	6.0	10.0	6.0	10.0	6.0	21.6	6.0	30.0	1.9	2.7	6.6	2.4	16.0	2.0	16.0	2.2

Table 3. Best fit points obtained by the NN method. Dimensions are given in milimeters.

	$\mathbf{MPP_1}$		$\mathbf{MPP_2}$		$\mathbf{MPP_3}$		$\mathbf{MPP_4}$		$\mathbf{HR_1}$		$\mathbf{HR_2}$		$\mathbf{HR_3}$		$\mathbf{HR_4}$	
	D_1	l_{I_1}	D_2	l_{I_2}	D_3	l_{I_3}	D_4	l_{I_4}	l_{N_1}	d_{N_1}	l_{N_2}	d_{N_2}	l_{N_3}	d_{N_3}	l_{N_4}	d_{N_4}
$\chi_1^2 = \mathbf{0.12}$	3.2	30.0	4.6	26.7	5.8	22.2	6.0	15.7	1.9	4.6	3.6	3.0	9.9	2.8	16.0	15.4
$\chi_2^2 = \mathbf{0.29}$	3.8	30.0	6.0	10.2	6.0	20.6	6.0	26.0	1.9	3.2	8.3	3.0	16.0	2.4	16.0	12.6
$\chi_3^2 = \mathbf{0.40}$	6.0	10.0	6.0	10.0	6.0	21.6	6.0	30.0	1.9	2.8	6.2	2.3	16.0	2.0	16.0	2.2

Table 4. Average absorption in frequency ranges for all the optimised solutions. Low stands for the frequency interval $100 - 400$ Hz, high for $400 - 1500$ Hz, and all $100 - 1500$.

	MCMC				**GA**				**NN**			
	χ_i^2	$\overline{\alpha}_{\text{low}}$	$\overline{\alpha}_{\text{high}}$	$\overline{\alpha}_{\text{all}}$	χ_i^2	$\overline{\alpha}_{\text{low}}$	$\overline{\alpha}_{\text{high}}$	$\overline{\alpha}_{\text{all}}$	χ_i^2	$\overline{\alpha}_{\text{low}}$	$\overline{\alpha}_{\text{high}}$	$\overline{\alpha}_{\text{all}}$
$i = \mathbf{1}$	0.12	0.37	0.83	0.73	0.12	0.38	0.83	0.73	0.12	0.38	0.83	0.73
$i = \mathbf{2}$	0.29	0.40	0.75	0.68	0.29	0.39	0.75	0.68	0.29	0.40	0.75	0.68
$i = \mathbf{3}$	0.40	0.43	0.62	0.57	0.40	0.42	0.62	0.58	0.40	0.40	0.62	0.57

mization methods, but large variations can be observed between those associated with different cost functions. The designs obtained from χ_1 focus on increasing absorption at mid and high frequencies, which can be easily done by adjusting appropriately the geometric parameters of the MPPs. Conversely, in the case of χ_2 and χ_3, where absorption at low frequencies is preferred, it is observed how mid and high frequencies are progressively compromised to favour it. The result is higher peaks at low frequencies at the expense of absorption in the resting frequencies, where some deep valleys appear centered at ~ 1000 Hz, in the case of χ_2, and ~ 550 Hz and ~ 1050 Hz, for χ_3. From Tab. 4, it can be concluded that, while the improvement may be worthy in the case of χ_2, the solution for χ_3 turns out to be less compelling.

Fig. 5 compares the efficiency of the three methods through the convergence of the solutions with the iteration number for one representative case, namely χ_2. For a total number of 3500 iterations, it can be clearly seen that GA and NN algorithms converge substantially faster than the MCMC routine, for which, as mentioned in section 3.1, the first $N_p/3$ iterations are dedicated to randomly scanning the parameter space. This is the reason why, for this method, a convergence pattern like the one exhibited by the GA and NN algorithms does not appear until iteration ~ 1000.

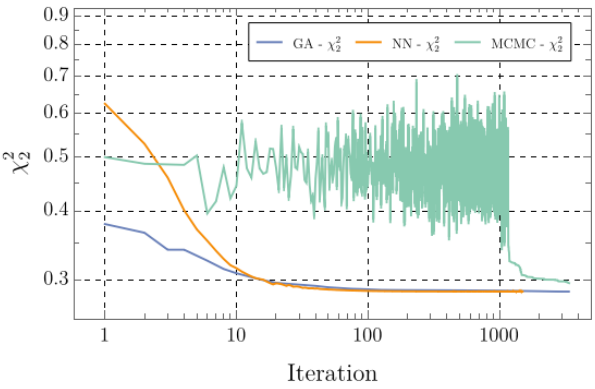

Figure 5. Convergence of the three methods for the χ_2 solution.

6. CONCLUSIONS

An acoustic metamaterial is developed and optimized to improve its absorption at low frequencies using three numerical methods and three distinct cost functions. While no substantial variations are found among designs obtained from different algorithms, significant modifications in the absorption take place when the cost function is altered. The maximum absorption in the whole range of frequencies is reached for a frequency-blind optimization although, in this case, frequencies below 400 Hz remain partially uncovered. The situation improves when considering a frequency-weighted cost function, but at the expense of reducing absorption in the total range of frequencies. The efficiency of the methods is discussed in terms of convergence of the cost function per iteration. GA and NN exhibit the best performance.

7. ACKNOWLEDGMENTS

This work has been partially supported by the Ministerio de Ciencia e Innovación, the Agencia Estatal de Investigación and the FEDER [Grant number PID2021-122237OA-I00], by project PID2023-148922OA-I00 (EEVOCATIONS) funded by MCIU/AEI/10.13039/501100011033 of the Spanish Government, and by project TEC-2024/COM-322 (IDEALCV-CM) by the Comunidad de Madrid.

8. REFERENCES

[1] K. Mahesh and R. Mini, "Theoretical investigation on the acoustic performance of helmholtz resonator integrated microperforated panel absorber," *Applied Acoustics*, vol. 178, p. 108012, 2021.

[2] J. H. Holland, *Adaptation in Natural and Artificial Systems*. The University of Michigan Press, 1st ed., 1975.

[3] D. E. Goldberg, *Genetic Algorithms in Search, Optimization and Machine Learning*. Addison-Wesley Publishing Company, 2nd ed., 1989.

[4] D. Bank, N. Koenigstein, and R. Giryes, *Autoencoders*, pp. 353–374. Springer International Publishing, 2023.

[5] L. Ardizzone, J. Kruse, S. Wirkert, D. Rahner, E. W. Pellegrini, R. S. Klessen, L. Maier-Hein, C. Rother, and U. Köthe, "Analyzing inverse problems with invertible neural networks," *arXiv preprint arXiv:1808.04730*, 2018.